Experimental Eye Research 115 (2013) 178–188

Contents lists available at ScienceDirect

Experimental Eye Research

journal homepage: www.elsevier.com/locate/yexer

A synthetic connexin 43 mimetic peptide augments corneal wound healing

Keith Moore [a,*], Zachary J. Bryant [a,1], Gautam Ghatnekar [b,c,2], Udai P. Singh [a,3], Robert G. Gourdie [d,4], Jay D. Potts [a,5]

[a] University of South Carolina School of Medicine, 6439 Garners Ferry Rd., Columbia, SC 29209, USA
[b] FirstString Research Inc., Mount Pleasant, SC 29403, USA
[c] Medical University of South Carolina, Charleston, SC 29425, USA
[d] Virginia Polytechnic and State University Carilion, 2 Riverside Circle Roanoke, Roanoke, VA 24016, USA

ARTICLE INFO

Article history:
Received 14 December 2012
Accepted in revised form 1 July 2013
Available online 20 July 2013

Keywords:
cornea
wound healing
sustained delivery
connexin 43
microencapsulation

ABSTRACT

The ability to safely and quickly close wounds and lacerations is an area of need in regenerative medicine, with implications toward healing a wide range of tissues and wounds. Using an in vivo corneal injury model, our study applied a newly developed peptide capable of promotion of wound healing and epithelial regeneration. The alpha-carboxy terminus 1 (αCT1) peptide is a 25 amino acid peptide from the C-terminus of connexin 43 (Cx43), modified to promote cellular uptake. Previous studies applying αCT1 to excisional skin wounds in porcine models produced tissues having an overall reduced level of scar tissue and decreased healing time. Rapid metabolism of αCT1 in previous work led to the investigation of extended release on wound healing rate used in this study. Here we delivered αCT1 both directly, in a concentrated pluronic solution, and in a sustained system, using polymeric alginate-poly-l-ornithine (A-PLO) microcapsules. Cell toxicity analysis showed minimal cell-loss with microcapsule treatment. Measurement of wound healing using histology and fluorescence microscopy indicated significant reduction in healing time of αCT1 microcapsule treated rat corneas compared with controls (88% vs. 38%). RT-PCR analysis showed an initial up regulation followed by down regulation of the gene keratin-19 (Krt19). Zonula occludens 1 (ZO-1) showed an opposite down regulation followed by an up regulation whereas Cx43 showed a biphasic response. Inflammatory indexes demonstrated a reduction in the inflammation of corneas treated with αCT1 microcapsules when compared with pluronic gel vehicle. These results suggest αCT1, when applied in a sustained release system, acts as a beneficial wound healing treatment.

1. Introduction

The ability to heal native corneal tissue would alleviate side effects such as infection and keratoplasty as well as the need for donor tissue (Aomatsu et al., 2012; Fukuda and Sasaki, 2012; Grupcheva et al., 2012; Karamichos et al., 2011; Lu et al., 2012; Shi et al., 2012; Shimmura et al., 2005; Trinkaus-Randall and Nugent, 1998; Yao et al., 2012). The cornea, with its avascular structure, follows a much different healing process than that seen in the skin. In the cornea a series of overlapping processes occur in a rapid fashion, beginning immediately after injury. Following epithelial injury, a cascade of cytokines (including IL-1 and PDGF) initiate keratocyte apoptosis (Wilson et al., 2001). Growth factor cytokines are then released by the lacrimal glands, which trigger keratocyte proliferation and migration from the stroma (Zeiske et al., 2001). This is followed by myofibroblast proliferation and migration to the wound site. Additional cytokines, such as TGFβ are released, triggering collagen production and remodeling (Netto et al., 2005). Inflammatory cells migrate to the wounded area and stromal remodeling occurs (Ye et al., 2000). As the epithelial layer completes closure the inflammatory cells undergo apoptosis and

Abbreviations: αCT1, alpha carboxy terminus 1; Cx43, connexin 43; Krt19, keratin-19; ZO-1, zonula occludens 1; $CaCl_2$, calcium chloride.

* Corresponding author. Tel.: +1 803 216 3838; fax: +1 803 216 3846.
E-mail addresses: moorekb@email.sc.edu (K. Moore), zachary.bryant@uscmed.sc.edu (Z.J. Bryant), ghatnekar@firststringresearch.com (G. Ghatnekar), udai.singh@uscmed.sc.edu (U.P. Singh), gourdier@vtc.vt.edu (R.G. Gourdie), Jay.Potts@uscmed.sc.edu (J.D. Potts).
[1] Tel.: +1 843 224 6674; fax: +1 803 216 3846.
[2] Tel.: +1 843 860 8372; fax: +1 843 720 3835.
[3] 300 West Coleman Blvd., Suite 203, Mount Pleasant, SC 29403, USA. Tel.: +1 803 216 3424; fax: +1 803 216 3847.
[4] Tel.: +1 540 526 2095.
[5] Tel.: +1 803 216 3820; fax: +1 803 216 3846.

0014-4835/$ – see front matter © 2013 Elsevier Ltd. All rights reserved.
http://dx.doi.org/10.1016/j.exer.2013.07.001

the keratocytes return to their original state (Wilson et al., 2001). The limbus of the corneal epithelium is a source of stem cells capable of transmigrational proliferation, but is not known to be necessary for reepithelialization after wounding (Dua et al., 2010). While the outline of the healing process is known, many of the details of the process and associated factors are still under investigation.

As a means of investigating the potential in vivo actions of αCT1 in corneal healing the Epithelial Mesenchymal transition (EMT) pathway was investigated here. EMT is a biological method of cellular rearrangement and repair of damaged tissue where immobile cells used for structural integrity and boundary formation may be mobilized to an area of need (Lee et al., 2006). Once the EMT process is complete the mesenchymal cells convert back to epithelial cells in the process called MET, or mesenchymal–epithelial transition. Typically the EMT process is tightly regulated by the body, as in embryogenesis (Radisky, 2005). The EMT process is not as well understood in the eye, with differing opinions on the extent of the relationship with wound healing. However, both Kawakita et al., 2012 and Aomatsu et al., 2012 were able to show the prevalence of EMT in the eye using cornea epithelial cells in relation to TGFβ and Slug signaling in recent studies. Similar results summarizing the occurrence of endothelial mesenchymal transitions in the cornea have been published as well (Lee et al., 2012), leading to the belief that may EMT play a role in the corneal healing.

The αCT1 peptide is a biotinylated 25 amino acid sequence, comprised of a 16 amino acid antennapedia domain, connected to a 9 amino acid (RPRPDDLEI) sequence from the C-terminus of Cx43 (Rhett et al., 2008, 2011). The cytoplasmic tight junction protein zonula occludens 1 (ZO-1) binds at its PDZ-2 domain with the DDLEI sequence of the Cx43 C-terminus end (Duffy et al., 2002). Previously Barker et al. (2002) found that intact ventricular myocardium exhibited a low level of ZO-1-Cx43 interaction. This interaction may be disrupted, leading to changes in protein–protein interactions which affect formation of gap junctions. Connexins play a key role as mediators of both cell growth and death and function in immune response, hematopoiesis, and development of progenitor cells (Herve et al., 2004; Oviedo-Orta and Evans, 2004; Vinkin et al., 2011). Binding of the C-terminus of Cx43 to ZO-1 is believed to affect cellular communication and gap junction remodeling in wound healing (Soder et al., 2009). αCT1 competitively inhibits this binding (Hunter et al., 2005; Soder et al., 2009), increases the rate of wound healing, and when applied to in vivo models reduced scar tissue formation in multiple wound healing models including cardiovascular injury, biomedical device implantation, and excisional skin wound models (Ghatnekar et al., 2009; O'Quinn et al., 2011; Soder et al., 2009). Barker et al. 2002 also developed a control peptide with the active C-terminus 9 amino acid sequence reversed while the inactive 16 amino acid antennapedia portion was left unchanged. While these results are promising, αCT1 showed a rapid metabolism rate in previous studies (<2 h). As a result we synthesized microcapsules capable of extending release of αCT1 over 48 h to determine therapeutic potential.

Previous studies from our laboratory using alginate poly-l-ornithine and alginate poly-L-lysine microcapsules loaded with 200 μM concentrations of αCT1 detailed the release profiles of the microcapsules (Moore et al., 2013). Release characteristics were adjusted using different polymer coatings and reduction in pore size by adjusting pH to 4.3 from a biologically neutral 7.4. Electrospray microencapsulation uses a voltage differential between a positively charged syringe attached to a high voltage generator and a grounded material, such as a crosslinking gelling bath. A device to control flow rate, such as a syringe pump, passes a polymeric material through the voltage field, which overcomes the surface tension force to produce droplets of a specific size (Chakraborty et al., 2009; Enayati et al., 2011). Here we apply identically synthesized peptide loaded capsules to a corneal wound model.

2. Materials and methods

2.1. Surgical creation of corneal wounds and post surgical treatment

Male Sprague–Dawley rats (Harlan Laboratories) (~240–260 g) were given food and water ad libitum. All experiments were carried out in compliance with the University of South Carolina Animal Resources Facility guidelines and Guide for the Care and Use of Laboratory Animals by the National Academy of Sciences. Prior to surgery, rats were placed under anesthesia using 60 mg/kg Ketamine, 7.5 mg/kg Xylazine, and 1 mg/kg Acepromazine. Two drops of a topical anesthetic, Alcaine (Alcon Canada, Mississauga, Canada) were applied to each eye, then wicked with a sterile ophthalmic sponge (Merocel, Beaver-Visitec International). A 5 mm trephine was placed on the surface of the cornea and two drops of 20% isopropyl alcohol were placed on the cornea surface for exactly 30 s. Care was taken to wound only the central cornea, excluding damage to the surrounding limbus. Exposure to the alcohol solution created a loosened 5 mm area of corneal epithelium, which was removed by gentle scraping under a dissecting microscope, leaving the exposed stromal layer. The cornea was then rinsed with 1% saline and wiped with an ophthalmic sponge to remove any remaining loose epithelium.

Post surgery, rats were placed into one of five time point groups spanning a one month period; 1 day, 3 days, 10 days, 21 days or 30 days. These five time points were repeated for four separate treatments with a total of 100 rats used in the study (25 per treatment/5 per time point). At each time point a total of 10 eyes were used with identical treatment in both eyes of each rat to eliminate eye to eye cross contamination through the tear ducts. To ensure sustained delivery of peptide in the cornea, a pluronic gel carrier (Pluronic F-127, Sigma) was used at a concentration of 25% w/v. The pluronic solution remains liquid at 4 °C, but gels once in contact with the warm eye. Treatment groups were comprised of two controls (10 μl 25% pluronic gel or 10 μl of 150 μM reverse peptide/25% pluronic gel) and two treatments with αCT1 peptide (10 μl 150 μM αCT1/25% pluronic gel per eye or 150 μM αCT1 A-PLO microcapsules/10 μl 25% pluronic gel per eye). Each treatment was applied immediately after surgery (0 h), 24 h, and 72 h. All rats were ethically sacrificed at the designated endpoints.

2.2. Synthesis and release of αCT1 from A-PLO microcapsules

Sterile sodium alginate (Sigma–Aldrich catalog#A0682, high maluronic acid content, low viscosity) poly-l-ornithine (Alfa Aesar L-ornithine hydrochloride 99%) microcapsules were synthesized and release of αCT1 was measured according to a previously published protocol (Moore et al., 2013). All microcapsules were synthesized with a 2% alginate/0.5% PLO concentration and gelled in 0.15 M calcium chloride ($CaCl_2$) (Sigma–Aldrich) solution 12 min. Synthesis parameters were constant at a needle to working bath distance of 7 mm, a voltage of 6.0 kV, and a flow rate of 60 mm/h. Microcapsule solutions were buffered to pH 4.3 using 0.1 M HEPES and 0.1 M hydrochloric acid (HCL) to control pore size and release rate. A-PLO microcapsules were loaded with αCT1 according to previous studies (Moore et al., 2013), with an initial concentration of 200 μM. To determine the peptide release profile, synthesized capsules were rinsed three times in deionized water, incubated at 37 °C, and the released peptide concentration determined with a microBCA Assay kit (Thermo Scientific).

2.3. Cytotoxicity testing of microcapsules

Cytotoxicity of materials used for A-PLO microcapsule synthesis was tested using an XTT based In Vitro Toxicology Assay Kit (Sigma Aldrich) on Human Cornea Epithelial Cells (HCEC) (Gibco C-018-5C) according to manufacturer's instructions. A cellular optimization assay was run using a range of HCECs from 1×10^6 to 1 x 10^3 cells per well to determine the linear range of XTT reaction. Based on the results, 65,000 cells per well were seeded onto a 96-well plate in media containing DMEM/1%FBS, 50 μg/mL Gentamycin, 0.5% Penicillin, and 0.1% Amphocyterin B for 24 h. Cells were then treated with a mixture of media with 2% $CaCl_2$, 150 μM A-PLO microcapsules pH 4.2, 150 μM A-PLO microcapsules pH 7.2, or 150 μM 2% alginate microcapsules pH 7.2, and incubated 24 h. Cells treated with media alone served as a positive control, while cells treated with 2% Triton-X 100 (Sigma Aldrich) served as a negative control. After 24 h the cells were rinsed in media, and XTT was added to each well at a 0.33 mg/mL concentration in cell culture medium with 8.3 μmol/L phenazine methyl sulfate (Sigma Aldrich). Cells were incubated for 24 h and absorbance was read at 450 nm using a BioTek Synergy 2 spectrophotometer. Results are the average of six repeats from separate cell isolations and are reported as a percentage of the positive control following background subtraction of media only wells. Standard error and mean were analyzed and plotted using GraphPad Prism 5 software, with statistical analysis using one way ANOVA ($p < 0.05$).

2.4. Fluorescent wound imaging and evaluation of wound closure

To assess wound closure rates, 2 μl drops of Fluress (fluorescein sodium and benoxinate hydrochloride, Akorn Incorporated) GFP labeled fluorescent dye were placed on the wounded cornea and allowed to cover the eye surface. Excess dye was removed using a sterile ophthalmic sponge, leaving a thin coat on the corneal surface. Fluress coats the cornea and penetrates the injury site, but is rinsed from the intact cornea. Images were taken of the wounds at 0 h (immediately post surgery), 1 day, 3 days, 10 days, 21 days, and 30 days, using a Zeiss Lumar V12 fluorescence microscope with a 20× objective and 1.5× lens magnification. All images were taken immediately prior to application of treatments. Each wound site area was measured using Axiovision Release 4.8.2 software. The percent decrease in wound area was calculated for each trial and treatment by comparing differences in wound area between initial and final measurements taken at each time point. Graphing and statistical analysis for significance was performed using GraphPad Prism 5 software analyzing the percent difference vs pluronic treated control groups (two way ANOVA analysis) and Kaplan–Meier survival analysis (Mantel–Cox test).

2.5. Histology and inflammation score

At previously described post surgery time points, whole eyes were completely removed from the ocular cavity and immediately dissected to remove the cornea. A central strip was cut from the wounded section of the cornea and snap frozen using liquid nitrogen. Frozen strips were held at −80 °C for 3 h and cryosectioned using a Zeiss Microm HM 505N Cryostat. Cornea sections were air dried and H&E stained using a Leica AutoStainer XL. Images were taken at 10× and 40× magnifications using a Nikon SMZ 1500 light microscope. Slides were then blind scored for inflammation using a 0–10 scale based on a previously published protocol modified for corneal tissue (Singh et al., 2003). Each sample was analyzed for cell infiltration, breakage of epithelial cells, presence of vacuoles, and irregularities in cell shape. A score of 0–2 indicated no cellular infiltrates/intact epithelial layer, 2–4 few infiltrates/breakage in the epithelial layer, 4–6 many infiltrates/non-intact epithelium, and 6–10 represents highly inflamed tissue. As reference controls, corneas receiving no treatment were taken immediately post surgery, sectioned, and also scored with the treated samples. Statistical analysis was performed using a two-tailed student's *t*-test with $p < 0.05$ significant.

2.6. RT-PCR of epithelial–mesenchymal transformation pathway genes

Corneas were sectioned at 1, 3, and 21 days for each treatment. Entire corneas were cut into sections, with individual ¼ sections (see Fig. 1) placed in 1 mL of Trizol Plus RNA purification reagent (Invitrogen), and processed according to manufacturer's protocol. Extracted RNA was tested for quality and quantity using an Agilent 2100 bioanalyzer and Agilent RNA 6000 nano kit (Agilent Technologies, Inc.). Two random samples of RNA per treatment type were selected for each of the three (1, 3, 21 days) time points making sure no two RNA samples were selected from the same rat source in the same treatment group, using a sample labeling system. Samples were then converted to cDNA at 250 nM using a BioRad iScript cDNA kit (Bio-Rad Laboratories) according to manufacturer's instructions. Gene specific primers for Krt19, ZO-1, and Cx43 of the EMT pathway were designed using BLAST web based software and synthesized commercially by IDT technologies (Table 1). The gene attachment region binding protein (ARBP) was used as a calibrator reference. Primers were tested for efficiency using RNA from 3 day pluronic gel treated rats and optimized using PCR gel analysis (data not shown).

Real-time PCR was run with each gene according to a previously published protocol (Valarmathi et al., 2009) using a MyiQ single color real time PCR detection system (Bio-Rad Laboratories) with SsoAdvanced SYBR Green supermix, 3 pmol/rxn primers and 1 μl cDNA. All data were analyzed using the Relative Expression Software Tool (REST XL), with pluronic gel treated samples serving as the baseline control. Statistical analysis was performed using both the REST XL and GraphPad Prism data analysis software.

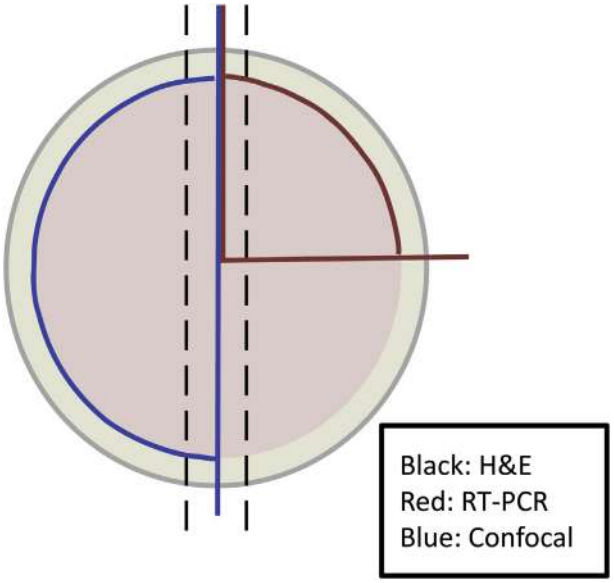

Fig. 1. Outline of corneal dissection. Half sections (blue) were used in confocal staining, ¼ sections (red) for RT-PCR and central strips (black) for H&E on different sample corneas. (For interpretation of the references to colour in this figure legend, the reader is referred to the web version of this article.)

Table 1
RT-PCR primer sequences.

Gene	Forward primer	Reverse primer	Product length (bp)
ARBP	5′-CGACCTGGAAGTCCAA CTAC-3′	5′-ATCTGCTGCATCTG CTTG-3′	109
Cx43	5′-TCAGCCTCCAAGGAGTTC CACCAAC-3′	5′-GCACTGACAGCCACAC CTTCCC-3′	159
Krt19	5′-AGCATGAAAGCTGCC CTGGAA-3′	5′-ATACTGCTGATCACACC CTGGA-3′	92
ZO-1	5′-CCATCTTTGGACCGATT GCTG-3′	5′-TAATGCCCGAGCTC CGATG-3′	123

2.7. Immunofluorescence staining and confocal microscopy

Whole eyes were removed and fixed in 2% paraformaldehyde at 4 °C for 24 h, then dissected from the eye to remove the cornea, cutting each into four equal ¼ sections (Fig. 1). Immunofluorescence preparation was performed and staining was carried out on single ¼ sections, including portions of the injury site, as previously described (Valarmathi et al., 2009). Primary antibody dilutions used for immunofluorescence staining are listed in Table 2. Staining was for 1 h at RT in the dark with the exception of DAPI (30 min) and anti-Cx43 (2 h). Alexa Fluor 488 (Molecular Probes, Invitrogen) secondary antibodies were added in dilutions of 1:100 in blocking buffer for 1 h at RT in the dark. Images were obtained with a Zeiss LSM 510 Meta CSLM microscope. Negative controls using only secondary antibodies were also performed.

3. Results

3.1. Microcapsule release and biocompatibility analysis

This study compared wound healing of a directly applied dose of 150 μM αCT1 vs. controlled αCT1 release through A-PLO pH 4.3 microcapsules at the same concentration. Previous studies using αCT1 showed the peptide was metabolized within 2 h of application in vivo (Rhett et al., 2011), leading to testing microencapsulation for sustained release. For proof of concept, FITC labeled αCT1 is shown microencapsulated in 180 μm microcapsules in Fig. 2A. A-PLO pH 4.3 microcapsules synthesized ([200 μM] initial) released an average of 113.99 ± 42.85 μM αCT1 over 48 h, shown in Fig. 2B. In these tests, the small size of αCT1 led to a rapid burst release of 80% of the αCT1 in the first two hours from 2% alginate microcapsules. Polymer coating of the 2% alginate with 0.5% poly-l-ornithine, combined with a reduction in pH to 4.3, led to a delay in release over 48 h, rather than an initial burst. All microcapsules in these results were synthesized at a 6.0 kV voltage/60 mm/h flow rate, and matched for use here.

To ensure microcapsule biocompatibility, we performed an XTT cytotoxicity assay using HCECs treated with A-PLO microcapsules at both neutral and acidic pH values, uncoated 2% alginate microcapsules pH 7.2, and 150 μM αCT1. In addition, a 2% solution of media/0.15 M $CaCl_2$ used in the microcapsule synthesis gelling bath was tested. The graph in Fig. 2C shows the cell optimization of XTT used to determine the ideal HCEC count (65,000 cells/well) based on the linear region. Treatment with the microcapsules from this study (A-PLO pH 4.2) and two additional microcapsule types (alginate alone and A-PLO pH 7.2) with variations in both pH and material type provided an examination of the in vitro cellular reaction of each of the synthesizing materials/solutions. Percent survival values shown in Fig. 2D were as follows; 2% $CaCl_2$ showed a 86.06 ± 1.73% survival, A-PLO pH 4.2 a 93.91 ± 1.21% survival, A-PLO pH 7.2 a 97.64 ± 1.57% survival, and 2% alginate microcapsules pH 7.2 a 96.64 ± 2.24% survival. Buffering the pH in A-PLO microcapsules from a neutral pH of 7.2 to an acidic pH of 4.2 showed a negative effect on cell survival, with a reduction of 3.73%. Comparatively, uncoated 2% alginate microcapsules showed a 2.44% higher survival rate at a neutral pH 7.2 than the A-PLO pH 4.2 capsules. The lowest survival percent was shown when a 2% $CaCl_2$ solution was tested.

3.2. Analysis of corneal wound closure

Having determined the optimal microcapsule profile and determined the biocompatibility of the encapsulating materials, we next sought to test them in an in vivo wound model. Cornea measurements of wound closure rates for all four treatments at each of the time points (post surgery, 1, 3, 10, 21, 30 days) were evaluated through imaging of GFP labeled Fluress ophthalmic dye. Using a Zeiss Lumar V12 stereomicroscope and Axiovision software, we measured wound area at each time. For each treatment 25 randomly selected eyes were measured. Our results indicated by the 10 day point, all wounds reached complete closure (day 10 shown in Fig. 3, while day 21 and day 30 not shown). Samples of these wound closure images are shown in Fig. 3A for day 0 (post surgery), day 1, and day 3, while the average measurements are listed in the table below. The table of results in Fig. 3A lists the percent change in wound area of the final day 1 or day 3 measurements subtracted from the initial day 0 measurements.

Examining the results in Fig. 3A, the largest change in wound closure rate occurred in the first 24 h. The αCT1 treatment group showed an average increase in wound closure of 31.92% vs. pluronic controls, while those receiving αCT1 A-PLO microcapsule treatments showed a 49.92% increase in wound closure. From the 24–72 h time points, αCT1 treated corneas saw an additional 17.40% increase in wound closure. The αCT1 A-PLO microcapsule treated corneas dropped below the rate of the direct αCT1 values at this 24–72 h time period, but still increased wound closure 10.16% faster than pluronic treatment. Based on the release profile of the A-PLO microcapsules, we found ~93% of encapsulated αCT1 was released within the first four hours, as shown in Fig. 2B. This was an improvement on the rapidly metabolized direct application of αCT1 shown in previous in vivo studies, (previously referenced) and believe accounted for changes in wound closure rates in A-PLO treatments. Graphical representation of the percent difference in wound closure of each treatment compared to pluronic controls is provided in Fig. 3B. Two way ANOVA analysis indicated significant increase in wound closure rates at 1 day for reverse, αCT1, and αCT1

Table 2
Primary antibodies used in confocal microscopy immunohistochemistry.

Primary antibodies	Dilutions	Manufacturer	Cat. #	Purpose of interest
Phospho-histone H3 (Ser28)	1:200	Cell signaling	9713	Cell migration
Anti-connexin 43, C-terminus	1:200	Millipore	MAB3067	Migrating cells in EMT
Anti-cytokeratin-19	1:50	Novus-Biologicals	422238	Migrating cells in EMT
TNF-α	1:100	Phar Mingen	554641	Inflammatory cytokine
Anti-mI-TAC (CXCL11)	1:100	R&D Systems	MAB572	Chemokine/activated T cells

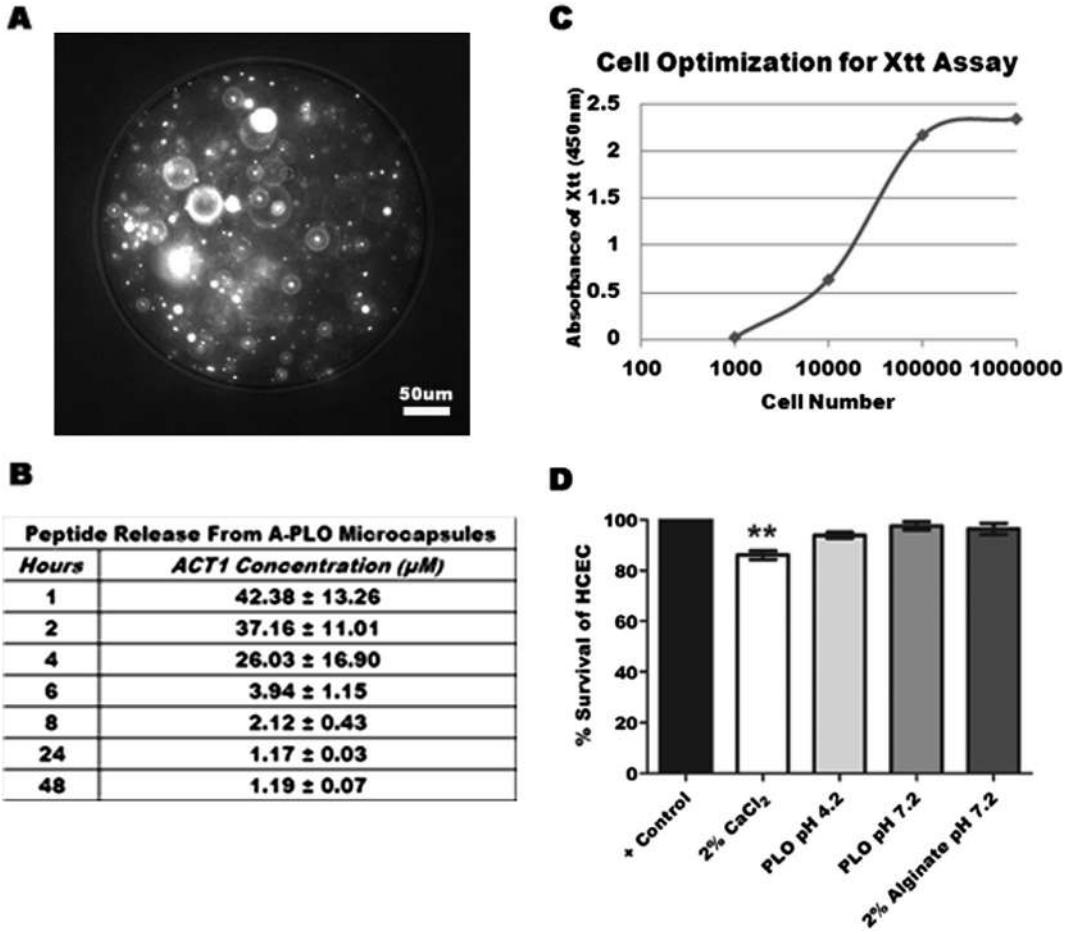

Peptide Release From A-PLO Microcapsules	
Hours	*ACT1 Concentration (μM)*
1	42.38 ± 13.26
2	37.16 ± 11.01
4	26.03 ± 16.90
6	3.94 ± 1.15
8	2.12 ± 0.43
24	1.17 ± 0.03
48	1.19 ± 0.07

Fig. 2. Summary of in vitro release and reactivity of alginate-polymer microcapsules. (A) 20× phase contrast image of microencapsulated FITC labeled αCT1 peptide. (B) Release profile of A-PLO microcapsules pH 4.3. Data represents four independent trials. (C) Cellular optimization graph using rabbit lens epithelial cells treated with XTT/PMS over 24 h. The linear region indicates optimal cells tested. (D) XTT cytotoxicity test results of polymeric microcapsules and calcium chloride on 65,000 HCECs. Results are the average of six trials.

microcapsule treatments. Significance continued with 3 day αCT1 microcapsule treatment only. Additional analysis using Kaplan–Meier survival analysis modified to examine open/closed wound states over 10 days for the four treatment groups is shown in Fig. 3C. Results further confirmed wound closure increased at rates exceeding control groups (pluronic 1.67%; control peptide 9.61%) when using both αCT1 (20%), and αCT1 microcapsule (20%) treatments by 3 days.

To further corroborate our wound closure data, samples of cornea from the 3 day time point were cryo-sectioned and H&E stained. These images indicated the epithelial layer was completely removed during surgery, exposing the stroma. We visualized the cell number of the new epithelial layers by examining the stained nuclei. Images taken at 40× magnification shown in Fig. 4B, D, F and H show that the epithelial layer reached ~4–5 cells thick by 3 days in regions of the cornea that have completely healed. Normal full thickness cornea has an epithelial layer 5–6 cells thick. Comparing the four treatment groups, there were no visible changes in the epithelial layer from treatment to treatment; i.e. increased layer thickness caused by treatment. Sample images of untreated cornea wounds taken immediately post surgery are shown along the wound edge (Fig. 4I (10×)) and within the wound margin (Fig. 4J (40×)). We concluded corneal healing approached both complete wound closure and full thickness reepithelialization at 3 days post surgery. Complete wound closure and full thickness reepithelialization were seen by 10 days post surgery (not shown).

To assess changes in the level of inflammation following treatment of the cornea we performed a blind inflammatory scale assessment. Both αCT1 treated and A-PLO αCT1 microcapsule treated were blind scored on a 0–10 inflammation scale against pluronic treated and untreated post surgical samples. Five randomly chosen slides of day 3 corneas were imaged from each of the four treatment groups and given a score based on the previously listed criteria. Fig. 4K indicates the average values of each score with SEM. Untreated post surgical control samples had an average score of 0.5, while pluronic treated averaged 8.18, indicating a high level of inflammation. The αCT1 treated (4.17) and A-PLO αCT1 microcapsule (4.73) samples showed moderate inflammation at 3 days. Statistical analysis indicated these values to be significantly less than pluronic controls in both cases.

3.3. Examination of wound healing response by RT-PCR and immunohistochemistry

The biochemical response of the wounds to treatment was analyzed by focusing on genes from the epithelial to mesenchymal transformation (EMT) pathway and those specific for the Cx43-ZO-1 interaction. Reepithelialization of the cornea involves gap junction and tight junction remodeling, thought to be affected by the presence of αCT1. Therefore, we hypothesized as corneal cells undergo remodeling and healing there would be a measureable change in EMT genes.

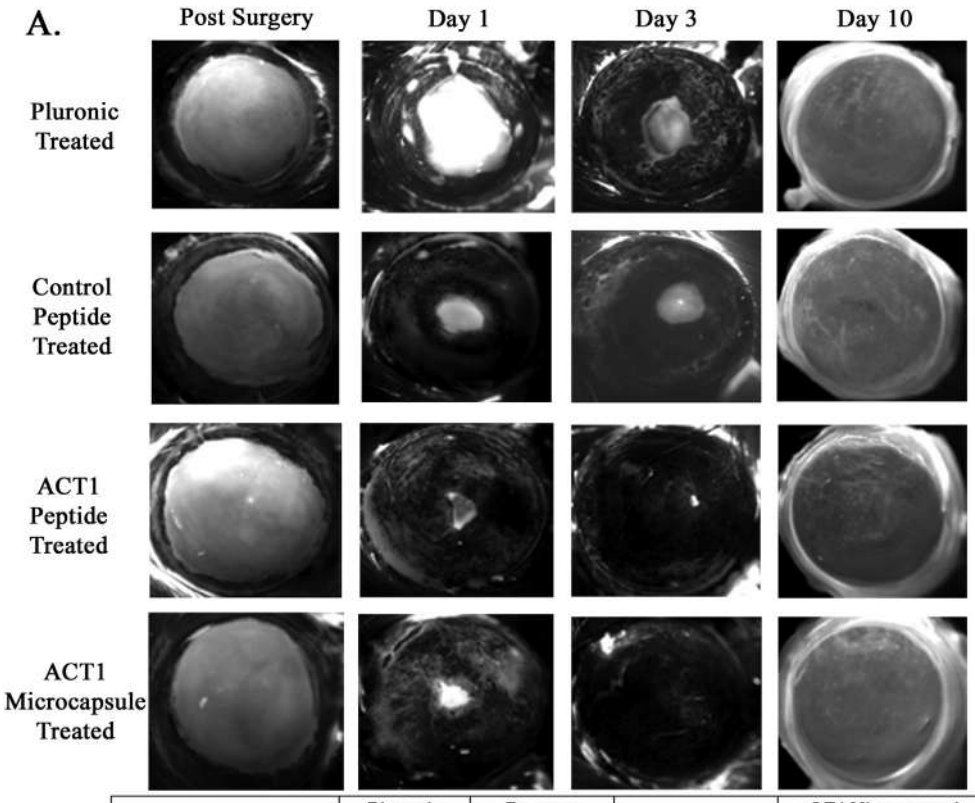

	Pluronic Treated	Reverse Treated	αCT1 Treated	αCT1 Microcapsule Treated
% change 0-24hrs	38.86 ± 27.12	52.32 ± 29.59	70.78 ± 22.43	88.78 ± 12.69
% change 24-72hrs	76.70 ± 19.60	89.59 ± 8.15	94.1 ± 10.08	86.86 ± 19.72
% change 0-72hrs	84.60 ± 15.19	94.93 ± 5.60	97.16 ± 4.93	99.15 ± 1.39

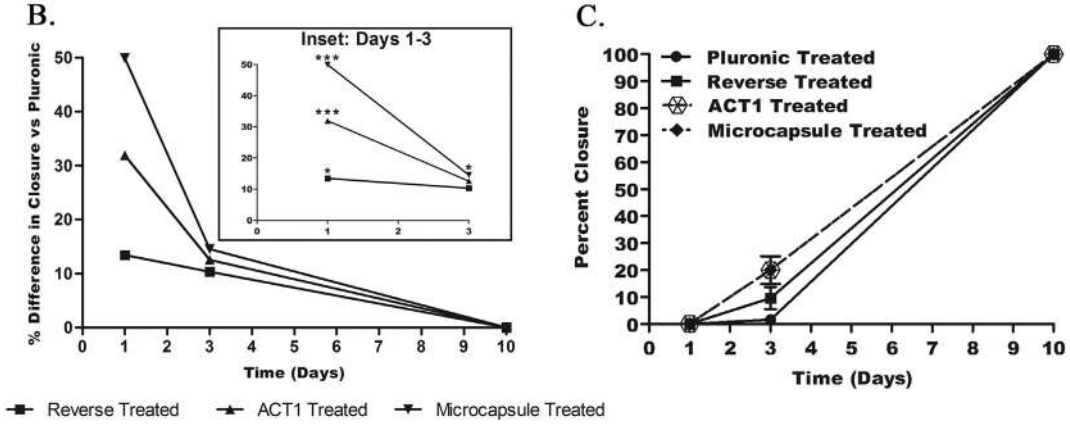

Fig. 3. Progressive wound healing over 10 days in a rat corneal injury model. (A) Fluress ophthalmic dye staining of corneal defects immediately after surgery. Repeated at 1 day, 3 days, and 10 days. Additional staining completed on days 21 and 30 (not shown). Treatments from top to bottom on each eye: 25% pluronic gel, 150 μM control peptide, 150 μM αCT1, and 150 μM A-PLO microencapsulated αCT1. Below is a summary of wound closure rates. (B) Analysis of the percent differences in wound closure of each treatment group compared to the values measured using the pluronic control group over 10 days. Statistical analysis by two way ANOVA ($p < 0.05$). (C) Kaplan–Meier analysis of wound closure examining the percent closure at 1, 3, and 10 days.

Genes for Cx43, Krt19, and ZO-1 were analyzed by RT-PCR at 1, 3, and 21 days using samples from all treatments. These time points were selected to analyze the immediate impact of the treatments (1 day), the impact at near wound closure (3 days), and the long term impact (21 days). The results are summarized in Fig. 5 using pluronic treated samples at each time point as baseline controls. On day 1, all treatments caused a down regulation of Cx43, with both αCT1 (−1.80) and A-PLO (−1.61) capsules less than the control treatment (−2.05). Cx43 is known to be down regulated immediately after a wound response, consistent with our data at 1 day. By day 3 all three treatment groups were up regulated in the Cx43 group (control: 1.12, αCT1: 1.60, and A-PLO: 1.50) with αCT1 treatment statistically significant ($p < 0.05$). The 21 day treatment group showed biphasic results between the control group and the two αCT1 treatments (control up 2.16 fold, αCT1 down 1.16 fold, and A-PLO down 1.31 fold). The results of ZO-1 at day 1 and 3 were consistent with the data for Cx43 in all treatment groups with down regulation at day 1 (control down 1.98 fold, αCT1 down 1.18

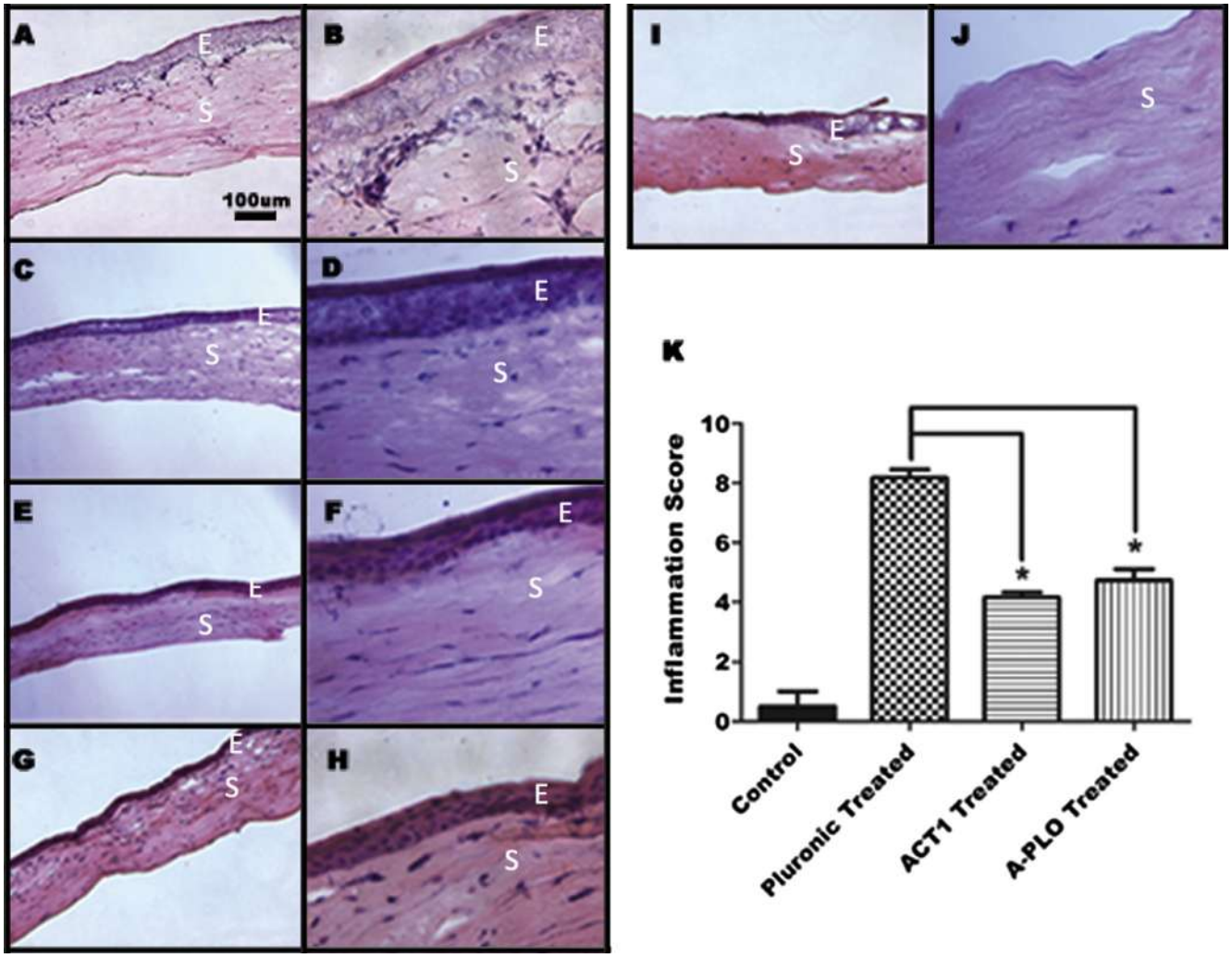

Fig. 4. Histological cryo-sectioning and staining of day 3 corneas using hematoxylin and eosin. Each row contains a representative cornea sample for each treatment at 10× magnification (left) and 40× magnification (right). (A, B) 25% Pluronic gel treated, (C, D) 150 μM control peptide treated (E, F) 150 μM αCT1 treated (G, H) 150 μM A-PLO microencapsulated αCT1 treated. Images I and J show a 10× (left) and 40× (right) time 0 untreated cornea for comparison. The images are labeled with *E*, to mark the epithelial layer, and *S* for the stromal layer. (K) Summary of inflammatory scoring for time 0 untreated control samples, pluronic, αCT1, and A-PLO αCT1 microcapsule treatments at day 3.

fold, and A-PLO down 1.44 fold) and up regulation at day 3 (control up 1.27 fold, αCT1 up 1.21 fold, and A-PLO up 1.24 fold). Our third examined gene, Krt19, is a stemness related marker thought to be down regulated during the EMT process, through roles in cell migration (Kong et al., 2010; Zhou et al., 2008). Aomatsu et al. (2012) were able to confirm down regulation of Krt19 using Snail and Slug overexpression in human corneal epithelial cells (Aomatsu et al., 2012; Ma et al., 2010). Here we show an immediate up regulation of Krt19 at day 1 in all treatments, with significance in both αCT1 (up 3.49 fold) and A-PLO treatment (up 2.57 fold) groups. By day 3 and continuing to day 21, Krt19 is consistently down regulated with significance shown with day 3 A-PLO treatment (down 3.66 fold).

Confocal microscopy using Krt19 (Fig. 6A and B) and Cx43 (Fig. 6C and D) was performed to validate the RT-PCR results. Fig. 6 shows sample images of day 1 and day 3 A-PLO treated corneal wounds. Arrows mark the reepithelializing wound margins in each image. Day 1 staining with Krt19 was expressed along the progressing wound edge as seen in Fig. 6A. Later time points with day 3 and day 21 (not shown) Krt19 staining showed little to no presence in all images. Cx43 antibody staining also produced staining similar to the results seen in the RT-PCR data. Minimal Cx43 staining is shown in Fig. 6C at day 1, while abundant within and around the wound margins at day 3, as viewed in Fig. 6D. This data further confirms our results for day 1 and day 3 Cx43 and Krt19, shown in Fig. 5.

3.4. Corneal response to A-PLO microcapsules

Treatment with αCT1 A-PLO microcapsules increased the rate of wound closure, but initially created a minor inflammatory response during healing in a small number of treated rats. Examples of the regions of affected tissue are shown in the upper and lower left images of Fig. 7. The resulting tissue was first seen in day 3 corneas with minimal to no presence at day 30. Samples of corneal tissue exhibiting this affected tissue were stained for the inflammatory markers TNF-α and ITAC (CXCL11). CXCR3 (chemokine C-X-C motif receptor 3) is a receptor expressed during inflammatory responses and associated with activated T cells as well as NK cells (Ondeykal et al., 2005). ITAC is an associated chemokine, active in the regulation of CXCR3 and up regulated during immune response. TNF-α, along with IL-6 and IL-1, is a well known pro-inflammatory cytokine and marker of immune response. Smooth muscle actin staining served as a cytoskeletal structural marker. The pro-

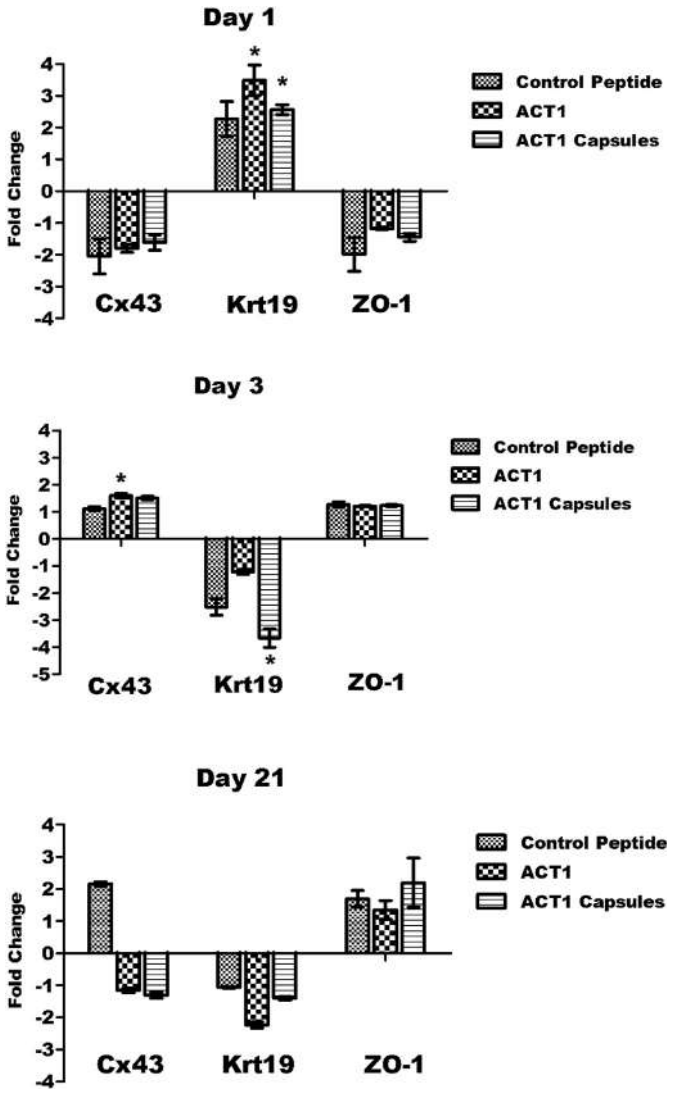

Fig. 5. RT-PCR analysis of corneas for gene expression of Cx43, Krt19, and ZO-1. Each time point is represented in the corresponding graphs for day 1 (top), day 3 (middle) and day 21 (bottom). Pluronic treated corneas serve as the baseline control, with the data presented for the up and down regulation of control peptide treated, αCT1 treated, and αCT1 A-PLO microcapsule treated samples.

inflammatory markers shown in Fig. 7A (TNF-α) and Fig. 7B (ITAC) were both expressed in tested corneas at 3 days with reduced presence by 30 days (not shown). Comparing the results shown here with the cytotoxicity data from Fig. 2D we saw a different response in vivo and in vitro to A-PLO microcapsules pH 4.2. Additional rats were tested with either 10 μL drops of 0.15 M $CaCl_2$ or 10 μL aliquots of triple DI water rinsed A-PLO pH 4.2 microcapsules. Only rats receiving the $CaCl_2$ treatment continued to exhibit the inflammatory response. We feel that the natural progression of the corneal injury coupled with residual $CaCl_2$ applied to the wound with the A-PLO microcapsules during treatment produced the inflammatory response. Subsequent corneal injury studies performed in the laboratory did not produce any inflammatory reaction with microcapsule treatment when extensively rinsed with deionized water prior to application in the eye.

4. Discussion

Examining the cytotoxicity of the A-PLO microcapsule synthesis related materials we found a high level of biocompatibility in vitro. Percent survival values using HCECs indicated a >93% survival with all materials (A-PLO pH 4.2, A-PLO pH 7.2, 2% alginate microcapsules pH 7.2, 150 μM αCT1) except 2% $CaCl_2$ which showed a 86.06 ± 1.73% survival. Buffering the pH in A-PLO microcapsules from a neutral pH of 7.2 to an acidic pH of 4.2 showed a small negative effect on cell survival, with a reduction of 3.73%. Comparatively, uncoated 2% alginate microcapsules showed a 2.44% higher survival rate at a neutral pH 7.2 than the A-PLO pH 4.2 capsules. The lowest survival percent was shown when a 2% $CaCl_2$ solution was tested. Based on this result, extensive washing of the $CaCl_2$ gelling solution from the microcapsules post synthesis is necessary when applying the microcapsules in vivo. As a result of >91% survival in all XTT trials, the A-PLO microcapsules were considered biocompatible for the corneal studies. The relatively small reduction in cell survival created by lowering the pH from 7.2 to 4.2, allowed for a high overall survival rate, while reducing the microcapsule pore size and extending αCT1 release.

The results of the wound closure analysis indicated controlled release of αCT1 over the first four hours enhanced the wound healing rate of the microcapsule treated corneas 18% over direct αCT1 treatment. Direct αCT1 treated corneas received a onetime peptide application to the wound of 150 μM, while microcapsule treated corneas received αCT1 release in the same dose for the full 24 h. At the 1 day point the rats in all treatment groups received a second treatment. It is thought that the first 24–36 h are the period when αCT1 is most functional in affecting gap junction formation in the healing wounds. As a result αCT1 treated corneas receiving a direct dosage of 150 μM of the peptide show a greater wound closure rate than A-PLO treated corneas receiving an extended amount of αCT1 over this 24–72 h time (i.e. directly applied αCT1 is actually more prevalent in the wound very early based on the slower release of the peptide from the microcapsules over 48 h). Additionally, a large standard error resulted when evaluating the 24–72 h period, which is thought to further account for differences in the direct αCT1 and A-PLO treatment final values. Looking at the total wound closure over the first 3 days (0–72 h) the αCT1 A-PLO microcapsule treatment showed the fastest overall wound closure speed, reaching nearly complete closure of 99.15% (14.55% faster than pluronic treatment) on average. This was followed by a 97.16% (12.56% faster than pluronic treatment) closure rate of αCT1. As a result, we hypothesize that αCT1 treatment by A-PLO microencapsulation leads to a faster wound closure rate for corneal wound injuries over the complete time period. While direct αCT1 treatment in the 24–72 h period is faster, the values indicated over the total 3 day time period showed a nearly complete closure (99.15%) when using A-PLO microcapsule treatment (Fig. 3A). Statistical analysis of the percent difference in wound closure measurements of each treatment vs. pluronic (Fig. 3B) and Kaplan–Meier analysis (Fig. 3C) confirmed the increased therapeutic potential of αCT1. At 3 days, as the wounds were reaching near closure, only microencapsulated αCT1 still produced wound closure rates significantly higher than controls. This indicated the advantage of using the controlled release system over direct application. Analysis using the Mantel–Cox test on the curves in the Kaplan–Meier graph (Fig. 3C) did not indicate significant differences between treated groups and controls. We believe the number of time points available for the curve did not allow for an accurate statistical comparison of the changes in wound closure. However, values seen at day 3 did indicate large differences in wound closure percent compared to controls, similar to data shown in Fig. 3B.

To examine inflammatory response of the cornea to treatment, αCT1 and A-PLO αCT1 microcapsule treated cyrosectioned samples were blind scored against pluronic treated and untreated post surgical samples. A significant decrease in inflammation was found

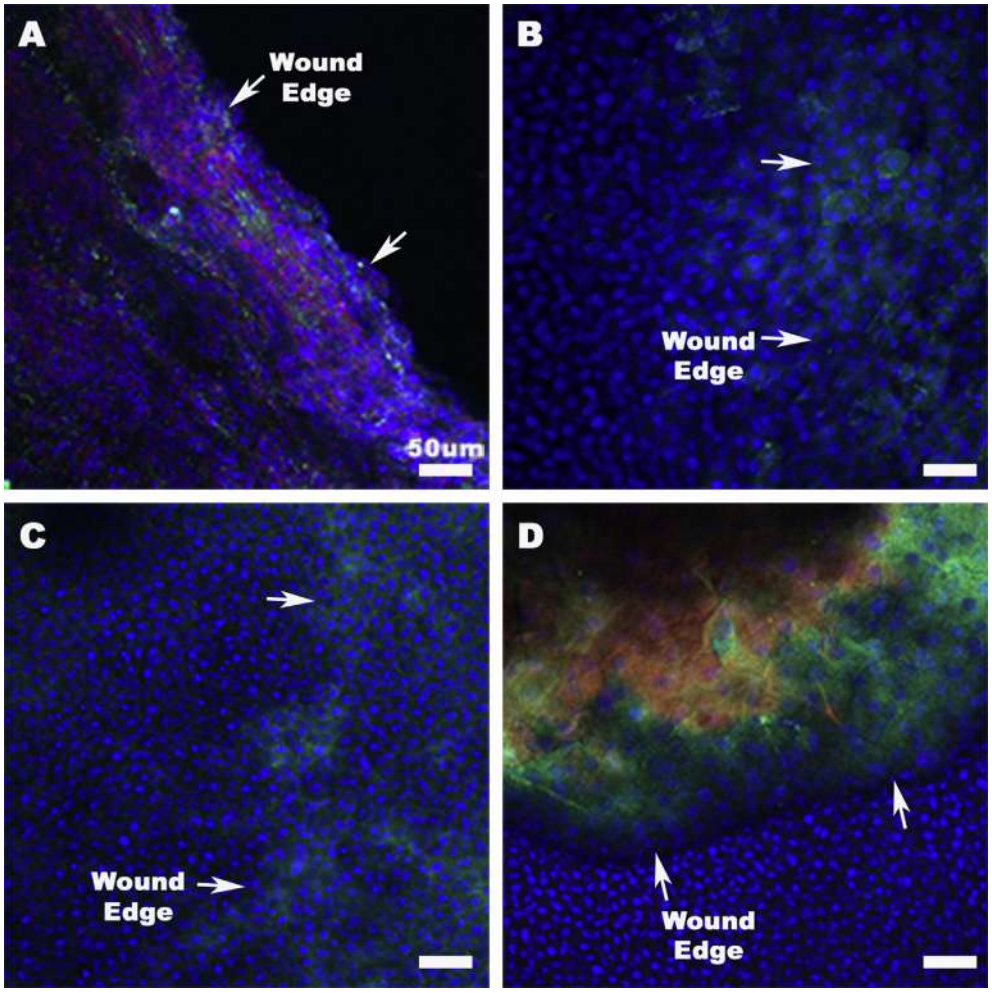

Fig. 6. Confocal microscopy of 1 day and 3 day cornea samples receiving treatment with αCT1 A-PLO microcapsules. All images are at a 20× magnification. (**A**) 1 day cornea: Blue-DAPI, Green-Keratin 19, Red-Phalloidin (**B**) 3 day cornea: Blue-DAPI, Green-Keratin 19, Red-Phalloidin (**C**) 1 day cornea: Blue-DAPI, Green-Connexin 43, Red-Phalloidin (**D**) 3 day cornea: Blue-DAPI, Green-Connexin 43, Red-Phalloidin.

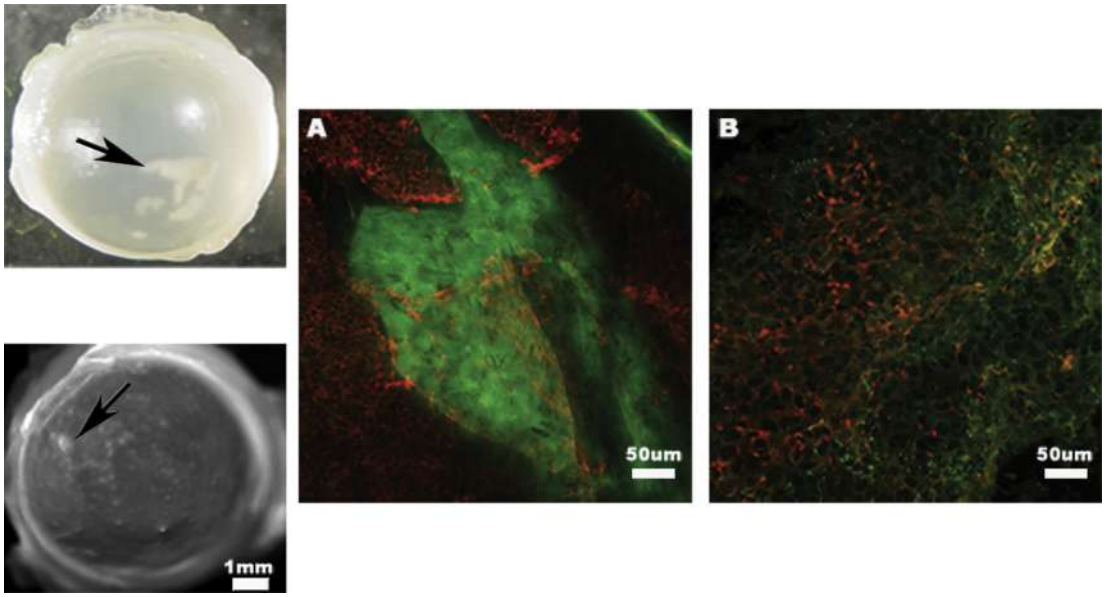

Fig. 7. The inflammatory response of the rat cornea to the αCT1 A-PLO microcapsule treatment in limited rats. Images are shown in both the upper left and lower left of the figure showing two representative portions of the affected tissue of the cornea at 30 days. (**A**) Confocal image at a 20× magnification of the affected tissue in a 3 day microcapsule treated cornea. Green-TNF-α, Red-smooth muscle actin. (**B**) 20× magnification of the affected tissue in a 3 day microcapsule treated cornea. Green-ITAC, Red-smooth muscle actin.

when compared to pluronic treated control samples. Inflammatory scoring was performed to ensure αCT1 treatment groups provided no additional inflammatory response exceeding that found in control groups. On the contrary we saw less inflammation at the 3 day mark with these treatments. The addition of αCT1 increased the wound healing rate, and therefore by the 3 day time point moved beyond the inflammatory stage of healing faster than pluronic treated samples. Coupled with the XTT cytotoxicity data, we found little negative compatibility issues when treating with αCT1 and A-PLO microcapsules in vivo. Previously published work using peptidomimetic sequences of connexins indicated a possible mechanism of action based on inflammatory suppression as a means of therapeutic action in models of spinal and cerebral injury (Danesh-Meyer et al., 2012; O'Carroll et al 2008). Additional work must be performed on the inflammatory reaction of αCT1 to further evaluate this reaction.

Barker et al. (2002) found in cardiac myocytes that Cx43 and ZO-1 were present in low amounts in normal tissue, but were expressed and co-localized upon tissue disruption. Here we show, through RT-PCR, a similar down regulation in corneal wound healing of ZO-1 consistent with typical Cx43 action. Between this 24 and 72hr time point, as the wound is healing, Cx43 and ZO-1 are up regulated as cell–cell adhesion and gap junction formation is recurring. By day 21 there was a departure from this consistency. The control group was shown to be up regulated in both Cx43 and ZO-1, while both αCT1 and A-PLO treatments showed Cx43 (down regulated) and ZO-1 (up regulated) no longer consistently co-expressed. While not statistically significant, this departure is of note.

The immediate up regulation in the RT-PCR data of Krt19 at day 1 is provocative, as the wound closure data shown in Figs. 3 and 4 indicated rapid reepithelialization. Down regulation of the gene at 3 and 21 days follows the known EMT patterns, as the wound continued closure and completion of healing of the multi-layered corneal epithelium. This data suggested immediately after wounding a transmigration stage of reepithelialization occurred, rather than an EMT proliferation of cells from the limbal region. Based on the levels of up regulation, Krt19, as well as other cytokeratins, play a role in the reepithelialization of corneal wounds. The treatment of corneal wounds with αCT1 is hypothesized to have resulted in an up regulation of migration of epithelial cells.

Finally we examined to minor response to A-PLO microcapsules in vivo looking at confocal immunohistochemistry of ITAC and TNFα. It is believed that a natural progression of the corneal injury coupled with residual $CaCl_2$ from the gelling bath applied to the wound with the microcapsules during treatment produced the inflammatory response in a small number of rats. This data is consistent with the results of the XTT cytotoxicity experiment previously listed. The results of subsequent corneal injury studies performed in the laboratory did not produce any inflammatory reaction with microcapsule treatment when the microcapsules were extensively rinsed with deionized water prior to application in the eye.

5. Conclusions

Treatment of corneal wound injuries with αCT1 peptide increased wound closure speed. The addition of a polymeric αCT1 A-PLO microcapsule system further increased the wound healing speed over αCT1 alone. Use of poly-l-ornithine as a polymeric drug delivery system was shown to be biocompatible, while the $CaCl_2$ gelling solution was found to be cytotoxic in vivo. Future use of this cationic crosslinking solution will require extensive washing with deionized water to ensure complete removal. Examination of Cx43 and ZO-1 in the corneal wound healing process showed results similar to previously published cardiac myocyte data, suggesting Cx43 and ZO-1 are coupled through down regulation immediately after injury or gap junction disruption, and are linked in up regulation during the healing process. Krt19 was shown to be significantly expressed 24 h after wounding with αCT1 and αCT1 A-PLO treatment. This EMT related protein may play a role in both migration of epithelial cells immediately after wounding and down regulation during a later EMT stage of cellular proliferation by day 3 post injury. Treatment with αCT1 may play a role in the early affects of migrational stages of corneal healing as well as EMT pathway genes.

Acknowledgments

We would like to acknowledge Dr. Ping Chen for her surgical assistance. Funding provided by NIH HL086901 (JDP) and First String Research, Inc.

References

Aomatsu, K., Arao, T., Abe, K., Kodama, A., Sugioka, K., Matsumoto, K., Kudo, K., Kimura, H., Fujita, Y., Hayashi, H., Nagai, T., Shimomura, Y., Nishio, K., 2012. Slug is upregulated during wound healing and regulates cellular phenotypes in corneal epithelial cells. Investigative Ophthalmology and Visual Science 53 (2), 751–756.

Barker, R., Price, R., Gourdie, R.G., 2002. Increased association of ZO-1 with connexin43 during remodeling of cardiac gap junctions. Circulation Research 90, 317–324.

Chakraborty, S., Liao, I., Adler, A., Leong, K., 2009. Electrohydrodynamics: a facile technique to fabricate drug delivery systems. Advanced Drug Delivery Reviews 61, 1043–1054.

Danesh-Meyer, H.V., Kerr, N.M., Zhang, J., Eady, E.K., O'Carroll, S.J., Nicholson, L.F.B., Cameron, C.S., Green, C.R., 2012. Connexin43 mimetic peptide reduces vascular leak and retinal ganglion cell death following retinal ischaemia. Brain–A Journal of Neurology 135 (2), 506–520.

Dua, H.S., Miri, A., Said, D.G., 2010. Contemporary limbal stem cell transplantation–a review. Clinical Experimental Ophthalmology 38, 104–117.

Duffy, H., Delmar, M., Spray, D., 2002. Formation of the gap junction nexus: binding partners for connexins. Journal of Physiology 96, 243–249.

Enayati, M., Ming-Wei, Chang, Bragman, F., Edirisinghe, M., Stride, E., 2011. Electrohydrodynamic preparation of particles, capsules, and bubbles for biomedical engineering applications. Colloids and Surfaces A: Physiochemical and Engineering Aspects 382, 154–164.

Fukuda, M., Sasaki, H., 2012. Quantitative evaluation of corneal epithelial injury caused by n-heptanol using a corneal resistance measuring device in vivo. Clinical Ophthalmology 6, 585–593.

Ghatnekar, G., O'Quinn, M., Jourdan, L.J., Gurjarpadhy, A., Draughn, R., Gourdie, R.G., 2009. Connexin43 carboxyl-terminal peptides reduce scar progenitor and promote regenerative healing following skin wounding. Regenerative Medicine 4 (2), 205–223.

Grupcheva, C., Laux, W., Rupenthal, I., McGhee, J., McGhee, C., Green, C., 2012. Improved Corneal Wound Healing through Modulation of Gap Junction Communication Using Connexin43-Specific Antisense Oligodeoxynucleotides. Investigative Ophthalmology and Visual Science 53 (3), 1130–1138.

Herve, J.C., Bourmeyster, N., Sarrouilhe, D., 2004. Diversity in protein-protein interactions of connexins: emerging roles. Biochimica et Biophysica Acta 1662, 22–41.

Hunter, A., Barker, R., Zhu, C., Gourdie, R.G., 2005. Zonula occludens-1 alters connexin43 gap junction size and organization by influencing channel accretion. Molecular Biology of the Cell 16, 5686–5698.

Karamichos, D., Hutcheon, A.E.K., Zieske, J.D., 2011. Transforming growth factor beta 3 regulates assembly of a nonfibrotic matrix in a 3D corneal model. Journal of Tissue Engineering and Regenerative Medicine 5 (8), 228–238.

Kawakita, T., Espana, E., Higa, K., Kato, N., Li, W., Tseng, S., 2012. Activation of Smad-Mediated TGF-b Signaling Triggers Epithelial–Mesenchymal Transitions in Murine Cloned Corneal Progenitor Cells. Journal of Cellular Physiology 228, 225–234.

Kong, B., Michalski, C.W., Hong, X., Valkovskaya, N., Rieder, S., Abiatari, I., Streit, S., Erkan, M., Esposito, I., Friess, H., Kleeff, J., 2010. AZGP1 is a tumor suppressor in pancreatic cancer inducing mesenchymal-to-epithelial transdifferentiation by inhibiting TGF-β-mediated ERK signaling. Oncogene 29, 5146–5158.

Lee, J., Dedhar, S., Kalluri, R., Thompson, E., 2006. The epithelial-mesenchymal transition: new insights in signaling, development and disease. The Journal of Cell Biology 172 (7), 973–981.

Lee, J., Ko, M., Kay, E., 2012. Endothelial mesenchymal transformation mediated by IL-1b-induced FGF-2 in corneal endothelial cells. Experimental Eye Research 95, 35–39.

Lu, H., Lu, Q., Zheng, Y., Li, Q., 2012. Notch signaling promotes the corneal epithelium wound healing. Molecular Vision 18, 403–411.

Ma, A., Zhao, B., Boulton, M., Albon, J., 2010. A role for notch signaling in corneal wound healing. Wound Repair and Regeneration 19, 98–106.
Moore, K., Amos, J., Davis, J., Gourdie, R.G., Potts, J., 2013. Characterization of polymeric microcapsules containing a low molecular weight peptide for controlled release. Microscopy and Microanalysis 19 (1), 213–226.
Netto, M.V., Mohan, R.R., Ambrósio Jr., R., Hutcheon, A.E., Zieske, J.D., Wilson, S.E., 2005. Wound healing in the cornea: a review of refractive surgery complications and new prospects for therapy. Cornea 24 (5), 509–522.
O'Carroll, S.J., Alkadhi, M., Nicholson, L.F.B., Green, C.R., 2008. Connexin43 Mimetic Peptides Reduce Swelling, Astrogliosis, and Neuronal Cell Death after Spinal Cord Injury. Cell Communication and Adhesion 15 (1-2), 27–42.
Ondeykal, J.G., Herath, K., Jayasuriya, H., Polishook, J., Bills, G., Dombrowski, A., Mojena, M., Koch, G., DiSalvo, J., DeMartino, J., Nanakorn, W., Morenberg, C., Balick, M., Stevenson, D., Slattery, M., Singh, S.B., 2005. Discovery of structurally diverse natural product antagonists of chemokine receptor CXCR3. Molecular Diversity 9, 123–129.
O'Quinn, M., Palatinus, J., Harris, B., Hewett, K., Gourdie, R.G., 2011. A peptide mimetic of the connexin43 carboxyl terminus reduces gap junction remodeling and induced arrhythmia following ventricular injury. Circulation Research 108, 704–715.
Oviedo-Orta, E., Evans, W., 2004. Gap junctions and connexin-mediated communication in the immune system. Biochimica et Biophysica Acta 1662, 102–112.
Radisky, D., 2005. Epithelial-mesenchymal transition. Journal of Cell Science 118 (19), 4325–4326.
Rhett, J.M., Ghatnekar, G.S., Palatinus, J.A., O'Quinn, M., Yost, M., Gourdie, R.G., 2008. Novel therapies for scar reduction and regenerative healing of skin wounds. Trends in Biotechnology 26 (4), 173–180.
Rhett, J.M., Jourdan, J., Gourdie, R.G., 2011. Connexin 43 connnexon to gap junction transition is regulated by zonula occludins-1. Molecular Biology of the Cell 22, 1516–1528.
Shi, L., Chang, Y., Yang, Y., Zhang, Y., Yu, Fu-Shin X., Wu, X., 2012. Activation of JNK Signaling Mediates Connective Tissue Growth Factor Expression and Scar Formation in Corneal Wound Healing. PLoS one 7 (2), 1–9.
Shimmura, S., Miyashita, H., Konomi, K., Shinozaki, N., Taguchi, T., Kobayashi, H., Shimazaki, J., Tanaka, J., Tsubota, K., 2005. Transplantation of corneal endothelium with Descemet's membrane using a hyroxyethyl methacrylate polymer as a carrier. British Journal of Ophthalmology 89, 134–137.
Singh, U.P., Singh, S., Taub, D.D., Lillard Jr., J.W., 2003. Inhibition of IFN-γ-Inducible Protein-10 Abrogates Colitis in IL-$10^{-/-}$ Mice. Journal of Immunology 171, 1401–1406.
Soder, B., Propst, J., Brooks, T., Goodwin, R., Friedman, H., Yost, M., Gordie, R.G., 2009. The connexin43 carboxyl-terminal peptide ACT1 modulates the biological response to silicone implants. Journal of the American Society of Plastic Surgeons 123 (5), 1440–1451.
Trinkaus-Randall, V., Nugent, M., 1998. Biological response to a synthetic cornea. Journal of Controlled Release 53, 205–214.
Valarmathi, M., Davis, J., Yost, M., Goodwin, R., Potts, J., 2009. A three-dimensional model of vasculogenesis. Biomaterials 30, 1098–1112.
Vinkin, M., Decrock, E., Leybaert, L., Bultynck, G., Himpens, B., Vanhaecke, T., Rogeirs, V., 2011. Non-channel functions of connexins in cell growth and cell death. Biochimica et Biophysica Acta 1818 (8), 2002–2008.
Wilson, S., Mohan, R., Mohan, R., Ambrósio Jr., R., Hong, J., Lee, J., 2001. The Corneal Wound Healing Response: Cytokine-mediated Interaction of the Epithelium, Stroma, and Inflammatory Cells. Progress in Retinal and Eye Research 20 (5), 625–637.
Yao, L., Li, Z., Su, W., Li, Y., Lin, M., Zhang, W., Liu, Y., Wan, Q., Liang, D., 2012. Role of Mesenchymal Stem Cells on Cornea Wound Healing Induced by Acute Alkali Burn. PLoS one 7 (2), e30842.
Ye, H.Q., Maeda, M., Yu, F.S., Azar, D.T., 2000. Differential expression of MT1-MMP (MMP-14) and collagenase III (MMP-13) genes in normal and wounded rat corneas. Investigative Ophthalmology and Visual Science 41, 2894–2899.
Zieske, J.D., Guimaraes, S.R., Hutcheon, A.E.K., 2001. Kinetics of keratocyte proliferation in response to epithelial debridement. Experimental Eye Research 72, 33–40.
Zhou, C., Nitschke, A., Xiong, W., Zhang, Q., Tang, Y., Bloch, M., Elliott, S., Zhu, Y., Bazzone, L., Yu, D., Weldon, C., Schiff, R., McLachlan, J., Beckman, B., Wiese, T., Nephew, K., Shan, B., Burow, M., Wang, G., 2008. Proteomic analysis of tumor necrosis factor-alpha resistant human breast cancer cells reveals a MEK5/Erk5-mediated epithelial-mesenchymal transition phenotype. Breast Cancer Research 10 (6), R105.